Time and Length Scales in Rotating Rayleigh-Bénard Convection

Yuchou Hu,[1,2] Robert E. Ecke,[1] and Guenter Ahlers[2]

[1]*Materials Division and Center for Nonlinear Studies, Los Alamos National Laboratory, Los Alamos, New Mexico 87545*

[2]*Department of Physics and Center for Nonlinear Science, University of California, Santa Barbara, California 93106*

(Received 28 November 1994)

We report experimental results for Rayleigh-Bénard convection of a fluid (CO_2) in a cylindrical cell with radius-to-height ratio 40 and rotated about a vertical axis. Near the critical rotation frequency for the Küppers-Lortz instability and for small $\epsilon \equiv \Delta T/\Delta T_c - 1$, we measured the frequency ω_a and the correlation length ξ of the pattern dynamics. They could be fit by power laws in ϵ only when exponent values much smaller than those predicted from amplitude equations were used. Alternately, the predicted exponents could be retained if the threshold were shifted to negative values of ϵ, thus yielding finite ω_a and ξ at onset.

PACS numbers: 47.20.–k, 47.27.–i, 47.32.–y

Spatiotemporal chaos in physical systems presents one of the exciting challenges in nonlinear science today [1]. The combination of spatial and temporal degrees of freedom has made such states extremely hard to characterize, both experimentally and theoretically. Often the experiments are possible only in regions difficult for theory to address, or theoretical models have no close experimental realizations. One system that seems particularly amenable to overcoming both of these problems is the Küppers-Lortz (KL) unstable state [2,3] in rotating Rayleigh-Bénard convection. This state, characterized by switching of local roll orientation by approximately 60°, has the attractive feature that it appears immediately at the onset of convection for arbitrarily small amplitudes provided the dimensionless rotation rate Ω is sufficiently large. This feature should make it theoretically more tractable than most other systems with spatiotemporal chaos since weakly nonlinear theory in the form of amplitude equations would be expected to be applicable. In addition, as a result of the local roll switching through a characteristic angle, one might expect this system to be in some sense somewhat more ordered than general spaitotemporal chaos.

An early theoretical description of the dynamics of the KL state by Busse and Heikes (BH) [4] was in terms of three coupled Landau-like amplitude equations in the rotating frame, corresponding to three modes with wave vectors advanced 60° with respect to each other in the direction of rotation. This model captured certain elements of KL convection. However, experiments [5–7] showed complex evolution of spatial domains, implying that the simple HB model was incomplete in an important way and that spatial effects needed to be incorporated in the theory. This was done by several authors [8–11], who added spatial gradient terms to the HB model and thus obtained three coupled real Ginzburg-Landau equations. They also developed generalized Swift-Hohenberg equations for the rotating convection problem. This theoretical work provided important predictions about the scaling of the switching time and the spatial domain size of the Küpper-Lortz unstable state. The amplitude equations predict that the characteristic time and spatial scales should vary as ϵ^{-1} and $\epsilon^{-1/2}$, respectively. Here $\epsilon \equiv \Delta T/\Delta T_c - 1$. These predictions are consistent with the generalized Swift-Hohenberg simulations [11], although the amount of simulation data seem to be insufficient at this time to infer precise exponents.

From an experimental perspective, no investigations have probed quantitatively length and time scales close to onset in large cells where intrinsic behavior unimpeded by the sidewalls might be expected. The results of Heikes and Busse [5,12] using shadowgraph visualization rather far from onset ($\epsilon > 0.5$) indicated an approximate scaling for the time scale of $\epsilon^{-3/4}$. No scaling for the length was presented in that work. A later study by Niemela and Donnelly [13] in a cryogenic fluid and a cell of modest aspect ratio (radius/height) $\Gamma \simeq 10$ yielded a characteristic time which scaled as $\epsilon^{-0.5}$. But as they had no visualization capabilities and thus could not determine the basic spatial state, the interpretation of this result is uncertain because other sources of time dependence such as the skewed-varicose instability are known to operate at low Prandtl number [14], and because for Γ as small as 10 it is known that domains are nucleated primarily at the sidewalls [15] rather than forming spontaneously in the cell interior. Thus, in our view the scaling of time near onset for the Küppers-Lortz instability has not been determined unambiguously, and nothing is known from experiment about the scaling of length.

We report on experimental characterizations of complex spatiotemporal dynamics in the Küppers-Lortz unstable region of Rayleigh-Bénard convection in a large aspect ratio cell ($\Gamma = 40$) close to onset ($\epsilon \leq 0.2$). We measured the convective heat transport, the averaged amplitude of the convective temperature field as reflected in the shadowgraph signal, the average switching angle Θ_{KL}, a correlation length (in units of d), and the average frequency ω_a (in units of t_v^{-1}, where $t_v \equiv d^2/\kappa$ is the vertical thermal diffusion time and κ is the thermal

 0031-9007/95/74(25)/5040(4)$06.00

diffusivity) as a function of ϵ for different dimensionless rotation rates $\Omega \equiv \Omega_D d^2/\nu$. Here Ω_D is the angular rotation speed in rad/s, d is the cell height, and ν is the kinematic viscosity. As had been found [14] for $\Omega = 0$, for small ϵ the convective temperature amplitude increased as $\epsilon^{1/2}$ and the convective heat current varied as ϵ. This is as expected for a forward bifurcation and in agreement with the amplitude equations which have been proposed for the rotating system. The switching angle Θ_{KL}, in good agreement with predictions [3], was $60° \pm 1°$ very near onset and decreased slightly with increasing ϵ. We found, however, that the ϵ dependence of ω_a was not consistent with the theoretically predicted ϵ^{-1} scaling for the time scale of Küppers-Lortz dynamics. The data were consistent with two possible scalings, either a power-law dependence with an exponent approximately equal to 0.6 or a functional form that implies a finite frequency at $\epsilon = 0$. Similarly, the correlation length, predicted to vary as $\epsilon^{-1/2}$, had either a power-law scaling with an exponent near 0.17 or again a form with a finite size at onset. These results indicate that the amplitude equations which have been proposed cannot explain quantitatively the Küppers-Lortz dynamics in our physical experiment. Our data provide important constraints on theoretical models and will, we hope, provoke new efforts to understand this important nonlinear system.

The experimental apparatus was described in detail elsewhere [14,16]. The cell bottom was an aluminum plate with a mirror finish, and the top was an optically flat sapphire window. The temperature of the bottom plate was measured with thermistors embedded in it, and a film heater, glued to the bottom of the lower plate, provided the heat current. The circular sidewalls were made of three layers of 0.34 mm thick cardboard paper with a straight vertical edge. The height of the cell, slightly uncertain because of an *in situ* adjustment of the cell flatness to ± 2 μm [17], was $d = 1.06 \pm 0.01$ mm. The cell was filled with CO_2 at 32 bars at a top-plate temperature of 33.7 °C. This sample had a Prandtl number $\sigma \equiv \nu/\kappa = 0.98$ and $t_v = 4.8$ s. Convection patterns were imaged using optical shadowgraph and digital signal processing techniques. The onset of convection was determined both from the convected heat flux and from the intensity of the shadowgraph images. Over the range $0 < \Omega < 22$, we found $1.49 < \Delta T_c < 2.19$. In all cases, the two determinations agreed to within $0.005\Delta T_c$ or better.

The data for the dynamics of the patterns were extracted from very many (about 100 000) shadowgraph images obtained for $\epsilon \lesssim 0.2$ and for $12 \lesssim \Omega \lesssim 22$. Representative examples for small ϵ and $\Omega = 17.6, 15.4$ and 12.1 are shown in Figs. 1(a), 1(e), and 1(g), respectively. The range of Ω is set to span the theoretically predicted [18] critical rotation frequency $\Omega_c \simeq 13$ for $\sigma \simeq 1$. The range of ϵ, on the other hand, was constrained on the high end by secondary instabilities, primarily by the skewed-varicose instability. The pattern dynamics consisted mostly of a switching of roll orientations through Θ_{KL}, and led to

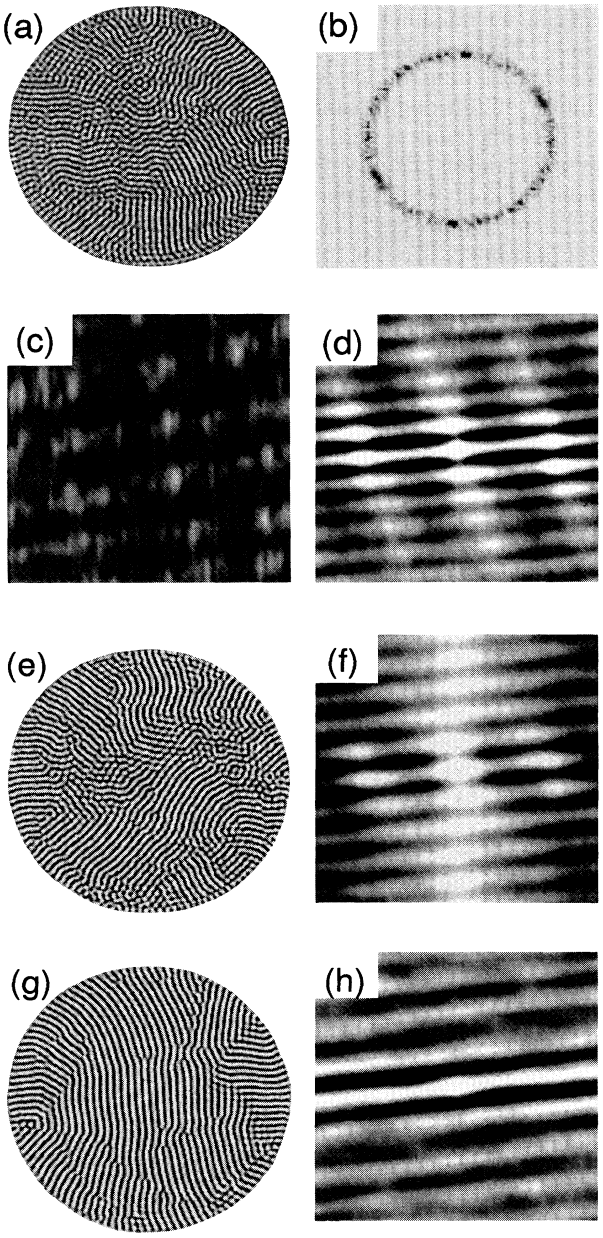

FIG. 1. Shadowgraph images $I(\mathbf{r})$ of convection patterns and their analysis. (a) $I(\mathbf{r})$ for $\Omega = 17.6$ and $\epsilon = 0.024$. (b) Grey-scale image of the modulus of the Fourier transform $F(\mathbf{k})$ of $I(\mathbf{r})$ shown in (a) (dark areas represent a large modulus). (c) $F(\Theta, t)$ [the average over k of $F(\mathbf{k})$] as a function of the azimuthal angle Θ of $\mathbf{k}$ (horizontal axis) and of time (vertical axis) in units of τ_v. Bright areas are high values of $F(\Theta, t)$. The image covers $0 \le \Theta \le \pi$ and $0 \le t \le 300$ (the actual run was much longer). (d) The angle-time autocorrelation function $C(\Theta, t)$ of $F(\Theta, t)$. The origin is at the center of the image. The angle (time) is shown in the horizontal (vertical) direction. The figure covers the range $-\pi/2 \le \Theta \le \pi/2$ and $-318 \le t \le 318$. (e) $I(\mathbf{r})$ for $\Omega = 1.54$ and $\epsilon = 0.054$. (f) $C(\Theta, t)$ as in (d), but for the conditions of image (e). The figure covers the range $-265 \le t \le 265$. (g) $I(\mathbf{r})$ for $\Omega = 12.1$ and $\epsilon = 0.058$. (h) $C(\Theta, t)$ as in (d), but for the conditions of image (g). The figure covers the range $-1060 \le t \le 1060$.

significant spatial and temporal correlations of these orientations. Thus one could use time sequences of the modulus of the Fourier transform $F(\mathbf{k}, t)$ to determine the temporal evolution of the dominant orientations. We determined $F(\mathbf{k})$ from the central parts of the images within 71% of the sample radius, using a Hanning window as described elsewhere [17]. The results thus are representative of the patterns in the cell interior well away from the walls [19]. As an example, $F(\mathbf{k})$ for the image in Fig. 1(a) is shown in Fig. 1(b). By averaging the square of $F(\mathbf{k})$ over the angular orientation Θ of $\mathbf{k}$, we obtained $F(\Theta)$ as a function of the angular orientation of $\mathbf{k}$. It typically showed three dominant orientations of rolls corresponding to the 60° Küppers-Lortz switching angle. By displaying many determinations of $F(\Theta)$ as a function of time one above the other, we constructed angle-time plots such as the one shown in Fig. 1(c) where time increases in the vertical direction and where the horizontal extent covers an angular range equal to π [the image in Fig. 1(a) yielded the top line of that plot, and only a small fraction of the actual run is shown]. Finally, we calculated the angle-time correlation function $C(\Theta, t)$ of $F(\Theta, t)$. For the conditions of Fig. 1(a) and for a time interval much shorter than the actual run, it is shown in Fig. 1(d). Here the equal-time, equal-angle point is in the center of the figure, and the horizontal Θ axis runs from $-\pi/2$ to $\pi/2$. Similar representation of $C(\Theta, t)$ for the conditions of the images in Figs. 1(e) and 1(g) are shown in Figs. 1(f) and 1(h), respectively. In the correlation function one can identify the switching angle Θ_{KL} as the angular distance between the bright (high-correlation) angular positions. The switching frequency ω_a is given by the inverse of the slope of the dominant bright lines in $C(\Theta, t)$.

At small ϵ and on the basis of the amplitude equations which have been proposed, we expect that $\omega_a \propto \varepsilon^1$ and that $\xi \propto \epsilon^{-1/2}$. Thus, we show in Fig. 2 the results for $1/\xi^2$ and ω_a as a function of ϵ for four representative rotation frequencies Ω. For the correlation length, we also show, as crosses, some results obtained [17] for $\Omega = 0$. Without rotation and over this ϵ range, the pattern consists of nearly straight parallel rolls [17]. Thus, the crosses reflect primarily the finite nature of the sample. Since they correspond to a length which is considerably larger than the lengths measured with rotation, it seems safe to conclude that finite-size effects in the analysis algorithm are not important. If the expected power laws were valid up to $\epsilon = 0.2$, the data should fall on straight lines. They show, however, significant curvature even for modest ϵ. In addition, any reasonable extrapolation to $\epsilon = 0$ leads to a finite value of ω_a and ξ at onset. Thus the data were fitted by the functions

$$\xi = \xi_0 \tilde{\epsilon}^{-1/2}(1 + D_\xi \tilde{\epsilon}),$$

$$\omega_a = \omega_{a0} \tilde{\epsilon}(1 + D_\omega \tilde{\epsilon}),$$

with $\tilde{\epsilon} = \epsilon + \epsilon_0$. The results are shown by the solid lines in Fig. 2. The fits gave distinctly negative values of ϵ_0.

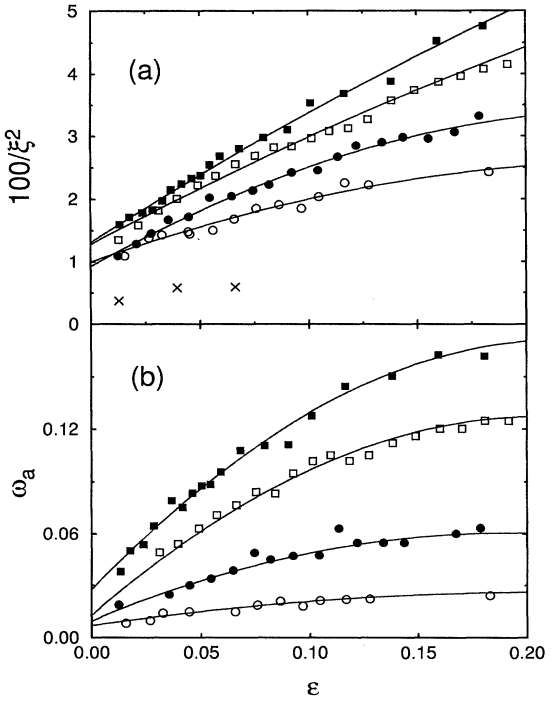

FIG. 2. (a) $100/\xi^2$ and (b) ω_a vs ϵ for different Ω. Solid squares: $\Omega = 17.6$. Open squares: $\Omega = 16.5$. Solid circles: $\Omega = 14.3$. Open circles: $\Omega = 12.6$. The solid lines are fits by polynomials in ϵ as described in the text. The crosses in (a) are of nearly straight parallel rolls at $\Omega = 0$.

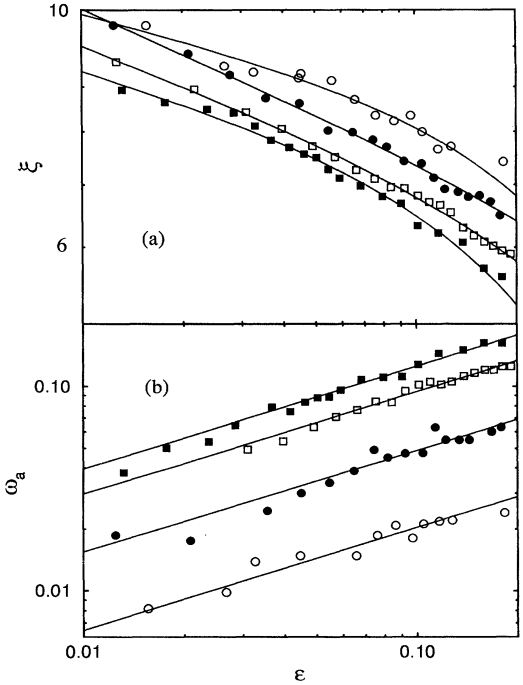

FIG. 3. Log-log plots of (a) ξ and (b) ω_a vs ϵ. The symbols and rotation frequencies Ω are as in Fig. 2.

The conclusion of this interpretation of the data, which retained the conventional exponents, is that the length and time scales at onset are finite.

Since the above interpretation of the data leads to conclusions which are contrary to what is expected, we search for an alternative explanation of the measurements. Figure 3 shows ξ and ω_a as functions of ϵ on logarithmic scales. The data for ω_a fall on straight lines, and thus can be represented well by the simple power law

$$\omega_a = \omega_{a,0}\epsilon^x.$$

The data for ξ show some curvature, but as shown by the solid lines, the power law with a higher-order correction term

$$\xi = \xi_0\epsilon^{-y}(1 + D_\xi\epsilon)$$

fits them well. This interpretation leads to a correlation length which diverges and a frequency which vanishes at onset, as was expected from the theory. The exponents, however, differ substantially from the expected values, as shown in the top panel of Fig. 4. There the open circles are for ω_a, and give $x \simeq 0.6$. The solid circles give $y \simeq 0.17$ for the exponent of ξ. We see that this interpretation of the measurements is also contrary to theoretical expectations.

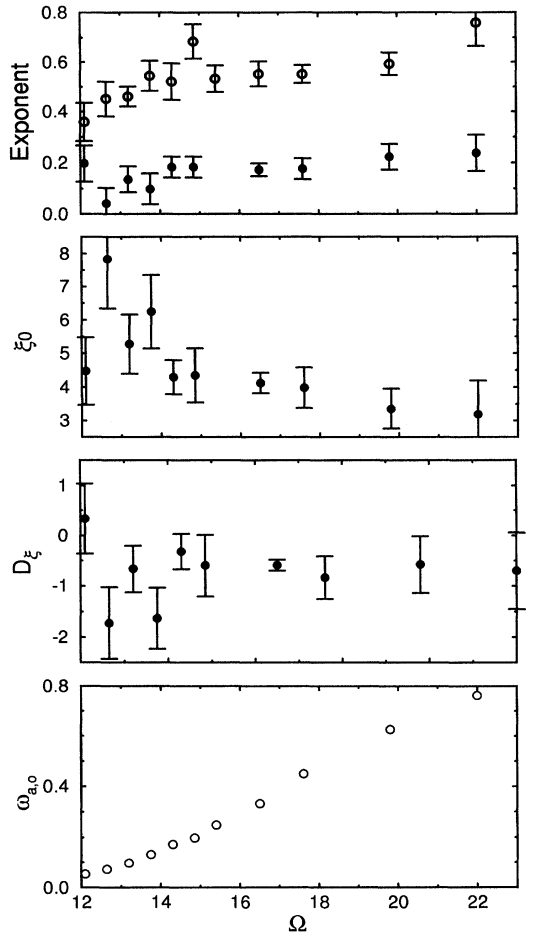

FIG. 4. Top panel: power-law exponents vs Ω for ξ (solid circles) and ω_a (open circles). The other three panels give the leading correlation-length amplitude ξ_0, the amplitude D_ξ of the correction term of the correlation length, and the leading amplitude $\omega_{a,0}$ of ω_a.

We conclude that the amplitude equations in their present form (which give $\xi \propto \epsilon^{-1/2}$ and $\omega_a \propto \epsilon^1$) are not consistent with the experimental measurements. It would be of interest to carry out more detailed numerical work using generalized Swift-Hohenberg equations with realistic sidewall boundaries in order to see whether the time and length scales of the experiment can be reproduced; despite eliminating commonly considered finite size effects as the explanation for our results, we cannot rule out more subtle influences of sidewall boundaries.

We would like to acknowledge helpful discussions with Mike Cross and Helmut Brand. This work was funded by the U.S. Department of Energy and by a UC INCOR Grant.

[1] For a recent review, see, for instance, M. C. Cross and P. C. Hohenberg, Rev. Mod. Phys. **65**, 851 (1993).
[2] G. Küppers and D. Lortz, J. Fluid Mech. **35**, 609 (1969).
[3] R. M. Clever and F. H. Busse, J. Fluid Mech. **94**, 609 (1979).
[4] F. H. Busse and K. E. Heikes, Science **208**, 173 (1980).
[5] K. E. Heikes and F. H. Busse, Ann. N.Y. Acad. Sci. **357**, 28 (1980).
[6] F. Zhong and R. Ecke, Chaos **2**, 163 (1992).
[7] E. Bodenschatz, D. S. Cannell, J. R. de Bruyn, R. Ecke, Y. Hu, and K. Lerman, G. Ahlers, Physics (Amsterdam) **61D**, 77 (1992).
[8] J. M. Rodríquez, C. Perez-Garcia, M. Bestehorn, M. Fantz, and R. Friedrich, Phys. Rev. A **46**, 4729 (1992).
[9] Y. Tu and M. Cross, Phys. Rev. Lett. **69**, 2515 (1992).
[10] M. Neufeld, R. Friedrich, and H. Haken, Z. Phys. B **92**, 243 (1993).
[11] M. Cross, D. Meiron, and Y. Tu (unpublished).
[12] K. E. Heikes, Ph.D. thesis, University of California, Los Angeles, 1979.
[13] J. J. Niemela and R. J. Donnelly, Phys. Rev. Lett. **57**, 2524 (1986).
[14] Y. Hu, R. E. Ecke, and G. Ahlers, Phys. Rev. E **48**, 4399 (1993).
[15] F. Zhong, R. Ecke, and V. Steinberg, Physics (Amsterdam) **51D**, 596 (1991).
[16] J. R. de Bruyn, E. Bodenshatz, S. W. Morris, S. Trainoff, Y. Hu, D. S. Cannell, and G. Ahlers (unpublished).
[17] Y. Hu, R. E. Ecke, and G. Ahlers (unpublished).
[18] The first calculation was reported by G. Küppers, Phys. Lett. **32A**, 7 (1970).The value quoted in this paper is from T. Clune and E. Knobloch (private communications).
[19] The results for ω_a and ξ with a Hanning window of 35% of the cell diameter do differ from those for the 71% window experimental and statistical uncertainty.
[20] S. W. Morris, E. Bodenshatz, D. S. Bodenshatz, D. S. Cannell and G. Ahlers, Phys. Rev. Lett. **71**, 2026 (1993).

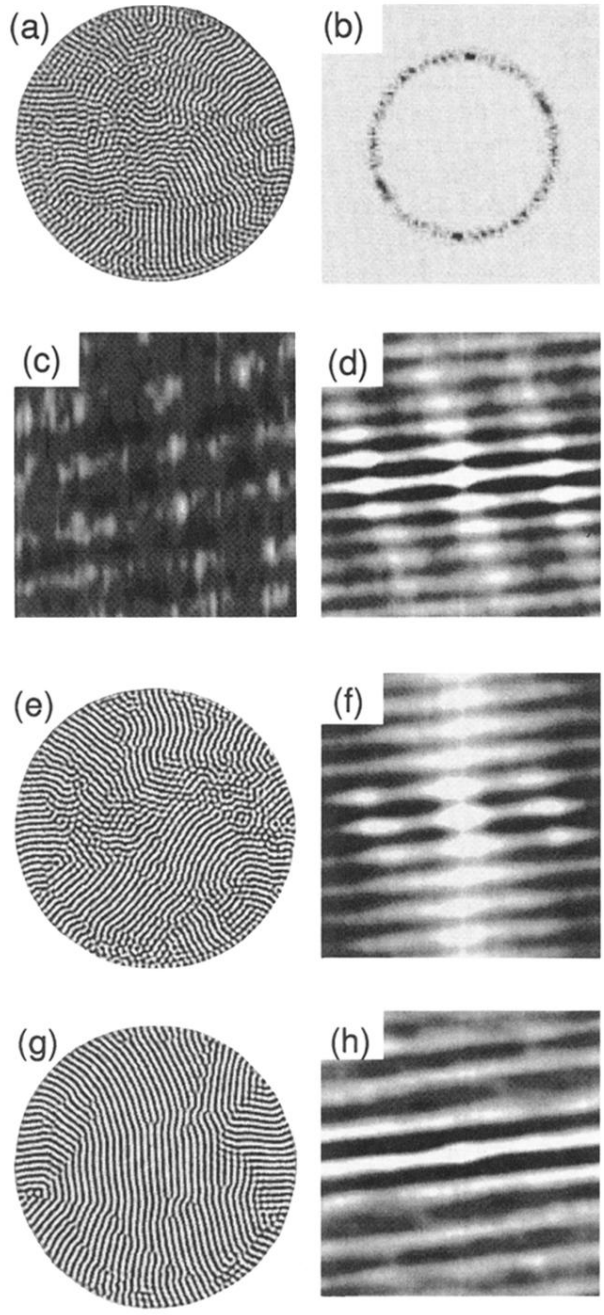

FIG. 1. Shadowgraph images $I(\mathbf{r})$ of convection patterns and their analysis. (a) $I(\mathbf{r})$ for $\Omega = 17.6$ and $\epsilon = 0.024$. (b) Grey-scale image of the modulus of the Fourier transform $F(\mathbf{k})$ of $I(\mathbf{r})$ shown in (a) (dark areas represent a large modulus). (c) $F(\Theta, t)$ [the average over k of $F(\mathbf{k})$] as a function of the azimuthal angle Θ of $\mathbf{k}$ (horizontal axis) and of time (vertical axis) in units of τ_v. Bright areas are high values of $F(\Theta, t)$. The image covers $0 \leq \Theta \leq \pi$ and $0 \leq t \leq 300$ (the actual run was much longer). (d) The angle-time autocorrelation function $C(\Theta, t)$ of $F(\Theta, t)$. The origin is at the center of the image. The angle (time) is shown in the horizontal (vertical) direction. The figure covers the range $-\pi/2 \leq \Theta \leq \pi/2$ and $-318 \leq t \leq 318$. (e) $I(\mathbf{r})$ for $\Omega = 1.54$ and $\epsilon = 0.054$. (f) $C(\Theta, t)$ as in (d), but for the conditions of image (e). The figure covers the range $-265 \leq t \leq 265$. (g) $I(\mathbf{r})$ for $\Omega = 12.1$ and $\epsilon = 0.058$. (h) $C(\Theta, t)$ as in (d), but for the conditions of image (g). The figure covers the range $-1060 \leq t \leq 1060$.